AIMS Materials Science, 9(4): 584–603.
DOI: 10.3934/matersci.2022035
Received: 17 February 2022
Revised: 01 April 2022
Accepted: 24 May 2022
Published: 02 Auguest 2022

http://www.aimspress.com/journal/Materials

Research article

Impact of polymer molecular weights and graphene nanosheets on fabricated PVA-PEG/GO nanocomposites: Morphology, sorption behavior and shielding application

Rusul A. Ghazi[1], Khalidah H. Al-Mayalee[2], Ehssan Al-Bermany[3,*], Fouad Sh. Hashim[3] and Abdul Kareem J. Albermany[4]

[1] Department of Medical Physics, Al-Mustaqbal University College, Babylon, Iraq
[2] Department of Physics, Faculty of Education for Girls, University of Kufa, Najaf, Iraq
[3] Department of Physics, College of Education for Pure Science, University of Babylon, Iraq
[4] Department of Physiology and Medical Physics, College of Medicine, University of Babylon, Iraq

* **Correspondence:** Email: ehssan@itnet.uobabylon.edu.iq; Tel: +964-780-4585050.

Abstract: Molecular weight (Mw) is an important feature that affects the physicochemical properties of polymers and their matrices. This study focused on the impact of increasing the Mw of polyethylene glycol (PEG) (4, 8 and 20 K) mixed with polyvinyl alcohol (PVA). Graphene oxide (GO) nanosheets were employed to reinforce the polymer matrix by aquatic mixing-sonication-casting to prepare the nanocomposites and investigate their optical properties. Fourier transform infrared spectroscopy revealed strong interfacial interactions among the components and successful fabrication of the nanocomposites. Optical microscopy and scanning electron microscopy confirmed the fine homogeneity of the polymers and the excellent dispersion of nanosheets in the matrix. The absorption peak was located in the ultraviolet region related to GO. PEG Mw and GO additive significantly improved optical properties such as absorbance, real and imaginary dielectrics and the absorption coefficient constant up to 75%, 40%, 120% and 77%, respectively. An enhancement in the optical properties was also observed after the energy gap values for allowed and forbidden transitions were improved up to 90% and 375%, respectively. These findings suggest the potential of these materials for several applications, such as in photovoltaic devices and heavy metal ion absorption for nuclear waste management.

Keywords: polymer molecular weight; graphene; PEG; optical properties; nanocomposite; radiation shield

1. Introduction

Graphene-based polymer nanocomposites have novel properties in addition to those conferred by their individual components [1,2]. Their significantly improved properties have opened up many promising applications for these materials. Nanotechnology is one of the preferred methods to improve a material's physical, mechanical and thermal properties. [3,4]. Another technique is the addition of nanofillers [5]. The carbon family has recently become a research focus, and graphene oxide (GO) has been used as an effective nanofiller to remove heavy metal ions from wastewater [6,7]. This compound also has critical applications in nuclear waste management because of its remarkable stability under complex conditions [8,9]. GO, a derivative of graphene, is a unique and impressive material containing functional groups with large surface areas and extended functional groups with their own features in addition to graphene's unique properties [10,11]. These properties make GO the most suitable to combine with a wide range of materials for improvement in their physical characteristics, such as optical, thermal, electrical and mechanical properties [12–14]. In the last decade, graphene polymer nanocomposites have become one of the best nanofillers because they exhibit excellent and unique properties for many applications [15,16].

Nanocomposite preparation is influenced by several factors, such as the component's properties, morphology, interfacial interaction, dispersion, homogeneity and loading transfer [17,18]. The polymer's molecular weight (Mw) significantly affects the polymer matrix's properties. Polymers have different Mws, and each Mw corresponds to a different application. This important factor has not been fully understood because of the lack of information and investigations.

Polyethylene glycol (PEG) is an essential polymer with significant applications and can exhibit various Mws; PEG with a high Mw is called poly (ethylene oxide) (PEO) [5,19]. PEG and poly(vinyl alcohol) (PVA) have substantial properties, such as high solubility, low toxicity, biocompatibility and rapid biodegradability in water [20]; and they contain important functional groups, such as one hydroxyl and carbonyl per unit of the chemical chain [21]. These functional groups improve the material's compatibility with many other polymers, fillers and nanofillers to manipulate or enhance the characteristics of materials and make them attractive to scientists, engineers and researchers [22]. The above polymers have been experimentally and theoretically investigated for numerous applications, such as in photovoltaic cells and devices, optics, optoelectronics and electronics [23–26]. However, their distinctive properties are related to their internal components, which differ from the polymer net [27]. Despite all the characteristics of pure and mixed polymers, they suffer from weakness in most of their optical properties due to structural defects [7,28].

Previous studies have focused on the electrical, mechanical, thermal and structural properties of only PVA or PEG alone or with graphene derivatives, GO or reduced GO. In addition to conduction, frequency, dielectric constants, thermal stability, strain, stress and other characteristics, Basha et al. [29] studied the effect of GO addition (from 0.1 to 0.3 g) on the optical characteristics of the polymeric mixture of poly(vinylpyrrolidone) (PVP) mixed with PVA as PVP/PVA-GO nanocomposites. The results showed that the highest concentration reduced the absorption edge and energy gap to 4.45 and 4.28 eV, respectively. Falqi et al. [30] described the thermal and mechanical

properties of PVA blends with PEG polymers prepared with various loading ratios of graphene (0.1–1 wt%) and found that the thermal properties exhibited good stability. Li et al. [31] considered the influence of added GO content on enhancing the thermal expansion and mechanical properties of PEGs with various Mws prepared using the solution method. The best effect was observed for the high-Mw PEG-20000, which exhibited strong interactions between the molecules of 20 K Mw PEGs and the functional groups of the GO nanosheets. Xiong et al. [32] described the influence of several low-Mw PEGs (200–6000 $g \cdot mol^{-1}$) with GO as a biosensor that detects profenofos in food, such as water and milk, in a single optical constant. GO/PEG nanocomposites with various Mws of PEG polymer showed the highest absorption for GO in the far ultraviolet (UV) region, which was less than 250 nm. The nanocomposite was also used for aptasensing assay to determine profenofos in tap water, milk and cabbage.

Despite all the previous studies [26,29–32], limited information is available on the relationship between the Mws and the interfacial interactions of low GO loading ratio and its effect on the morphology and optical properties of hybrid nanocomposites with PVA and PEGs of various Mws (4, 8 and 20 K). Therefore, this investigation addressed these essential factors. A mixing-sonication-casting method was developed and used to prepare PVA-PEG/GO nanocomposites. The structures and optical properties of the nanocomposites were investigated for the first time using different characterization techniques such as Fourier transform infrared (FTIR) spectroscopy, optical microscopy (OM), UV spectrophotometry and scanning electron microscopy (SEM).

2. Materials and methods

2.1. Materials

PVA with a −43.15 ℃ melting point and 99.8% purity was supplied by Panreac Company, Spain, and PEGs of 4000, 8000 and 20000 $g \cdot mol^{-1}$ were provided by Central Drug House, India. Graphite powder with a particle size of ≤40 μm for GO preparation, hydrogen peroxide, sodium nitrate, sulfuric acid with 99.8% purity, potassium permanganate and hydrochloric acid were purchased from Sigma-Aldrich Company, UK.

2.2. Preparation of GO

GO nanosheets were synthesized from graphite using the methods proposed by Hummer [5]. The characteristics of GO nanosheets are presented in Figure S1 of the supporting information.

2.3. Preparation of polymer matrix

Six different samples were prepared separately. First, 75 wt% PVA was mixed with distilled water (DW) using a magnetic stirrer at 70 ℃ for 60 min until complete dissolution. The temperature was then reduced to 40 ℃. Meanwhile, 24 wt% PEGs of three Mws were dissolved in distilled water. Three PVA/PEG samples were prepared by mixing PVA-DW with PEG-DW and stirring for 30 min. GO was first suspended in distilled water and then sonicated for 30 min for full dispersion before being loaded into polymer mixtures. Another three samples of PVA/PEG polymers were fabricated using the

above procedure and then loaded with 1 wt% GO to prepare the nanocomposites. After GO addition, the matrixes became fully homogeneous. The GO was fully dispersed in the matrix of the blended polymers after mixing for 96 h and sonication for 1 h. These processing methods are summarized in Table 1. All the matrixes were cast in a plastic petri dish at room temperature (RT) for 96 h under air to obtain dried films.

Table 1. Preparation of blended polymers and nanocomposites.

Sample code	Concentration (wt%)					Drying at room temperature
	PVA	PEG 4k	PEG 8k	PEG 20k	GO	
P1	75	24	-	-	-	Under air in a fume cupboard for 4 d
N1		24	-	-	1	
P2		-	24	-	-	
N2		-	24	-	1	
P3		-	-	24	-	
N3		-	-	24	1	

Equation 1, which represents transmittance (T), and Eq 2 were used to calculate the absorption coefficient (α) (cm^{-1}) [33].

$$T = \log A \tag{1}$$

$$\alpha = 2.303\ \text{Å/t} \tag{2}$$

where (A), and (t) represent the absorbance and the thickness of the sample, respectively. The extrapolated linear intercept of the curve with the energy of the photon (hυ) at $(\alpha h\nu)^n = (0)$ was used to calculate the allowed and forbidden indirect transitions of optical energy gap with Eq 3 [7].

$$ahv = B\left(hv - E_g\right)^n \tag{3}$$

where (B) is constant, (h) is Planck's constant, (v) is frequency, and the energy of phonon,(E_g) refers to the energy of the photon. The signs (-) and (+) represent the photon's activities of absorption and emission, respectively. (r) represents the exponential constant whose value is determined by the transition type. Here, r = 2 or 3 for the allowed direct and indirect transitions, respectively.

Equation 4 was used to calculate the refractive index value (n), which depends on the reflectance (R).

$$n = \frac{1+R}{1-R} + \left[\frac{4R}{(1-R)^2} - K^2\right] \tag{4}$$

$$K = \frac{\alpha\lambda}{4\pi} \tag{5}$$

where (λ) is the wavelength of the Cu Kα line (1.5406 Å), which was used to calculate the extinction coefficient (K). Equations 6 and 7 were used to estimate the real (ε_r) and imaginary dielectric constant (ε_i) for nanocomposites [33].

$$\varepsilon_r = (n^2 - k_o^2) \tag{6}$$

$$\varepsilon_i = (2nk_o) \tag{7}$$

Depending on the refractive index, polarizability (P) can be determined using Eq 8 [34].

$$P = \frac{3}{4\pi}\left(\frac{n^2-1}{n^2+1}\right) \tag{8}$$

Equation 9 was applied to estimate the optical conductivity (σ_{op}) [35].

$$\sigma_{op} = \frac{\alpha\, n\, c}{4\pi} \tag{9}$$

where (c) is the light velocity, and (α) is the absorption coefficient. The dielectric loss angle was calculated using Eqs 10 and 11 [36].

$$tan\,\delta = {}^{\varepsilon_i}/_{\varepsilon_r} \tag{10}$$

Loss angle was computed as

$$tan^{-1}\left({}^{\varepsilon_i}/_{\varepsilon_r}\right) = \delta \tag{11}$$

2.4. Characterization

The infrared spectra of the polymer blends/graphene nanocomposites were obtained using FTIR spectroscopy (Bruker, Germany) at 400–4000 cm^{-1}. An ultrasonic cleaner, model VGT-1613QTD with 60 W power and 40 kHz frequency, was used to exfoliate the GO nanosheets and achieve good dispersion in the polymer matrix. The surfaces of the films were characterized using a Nikon-73346 Optical Microscope (OM) from Olympus. The absorption spectra between the wavelengths of 300 and 1100 nm were obtained using a UV-1650 PC type Shimadzu by Phillips Company, Japan. The structures of the nanocomposites were characterized using an X-ray diffraction (XRD) instrument, Vertex 701, Shimadzu 600, from Japan. High-resolution images were captured at 10 kV using an Inspect S 50 SEM supplied by FEI Company.

3. Results and discussion

The blended polymers and nanocomposites were characterized using FTIR spectra between 400 and 4000 cm^{-1}, as shown in Figure 1. The characteristics of the absorption peaks of PVA and of $PEGs_{4k,\ 8k,\ 20k}$ as poly-blends with hybrid nanocomposites were found at 3283.45, 3219, 2917.99, 2882, 1732.87, 1720, 1620, 1466.01, 1360, 1341.57, 1240–1106.41, 1096.82, 1040, 961.86 and 841.42 cm^{-1}, which corresponded to the wide band of the –OH hydroxyl groups of the nanocomposite, stretching vibrations of the hydroxyl groups –OH of GO, symmetric stretching vibration band of $–CH_2$ methylene of PVA, asymmetric stretching vibration of $–CH_3$ methyl of PEGs, C=O stretching band of the carbonyl groups of the composite, C=O carbonyl groups at the GO nanosheet edges, C=C skeletal ring stretching vibration of GO, methylene –CH blending vibration of PEGs, primary or secondary, OH in-plan bending, methyl –CH asymmetric bending vibration of PVA, –OH group bending vibration of the nanocomposite, C–O stretching of poly(vinyl alcohols),

C–O–C epoxy group stretching vibration, C–O–C symmetric vibration and C–C group stretching vibration of PEGs, respectively [31].

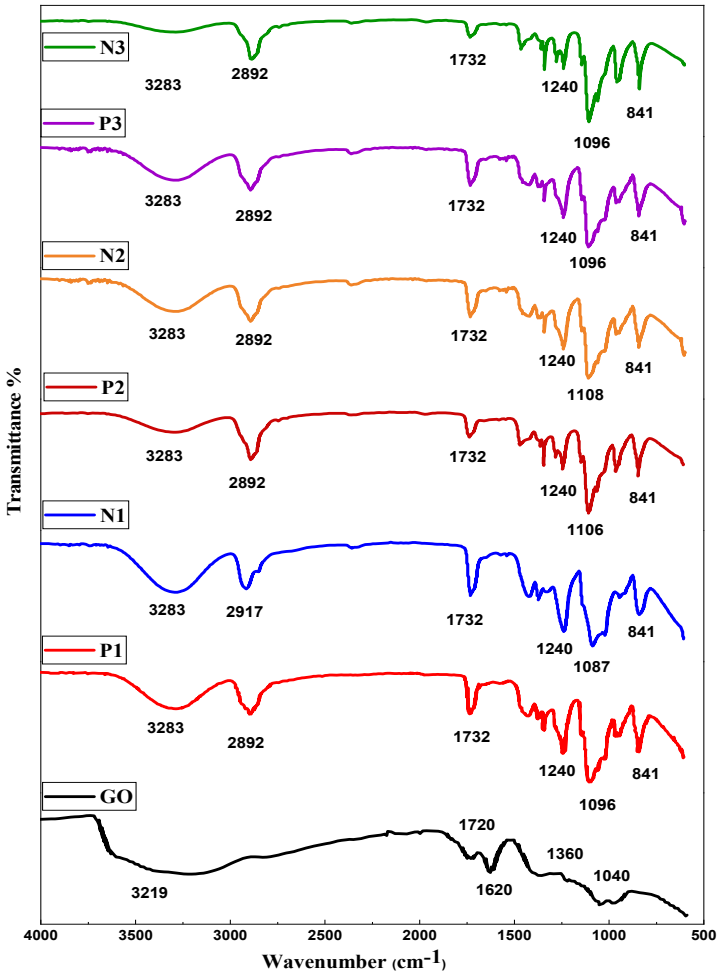

Figure 1. FTIR spectra of blended polymers and nanocomposites.

FTIR analysis of the nanocomposites revealed strong interfacial interaction bonds, particularly the –H bond, among the molecular chains of blended polymers and GO. When a small percentage of GO was added, a significant increase in intensity and a slight shift in peak positions at 1732 and 3283 cm^{-1} were observed. These findings were associated with the high solubility and good dispersion of the PVA/PEG polymer blend and the functional groups of GO. All these factors have led to the successful production of nanocomposites.

Figure 2 shows the XRD patterns of GO and P3 and N3 nanocomposites. The interlayer spacing pattern of GO was 0.79 nm, calculated at $2\theta = 11.1^{o}$ (002), which was in agreement with another finding [37]. PEG spectra revealed peaks at $2\theta = 19^{o}$, 23.3^{o} [38]. The PEG peaks revealed a slight shift in the 2θ peak of the N3 nanocomposites from 19^{o} to 18.9^{o}, which could be associated with the increment of interplanar crystal spacing. The lack of a GO peak could be attributed to the orientation of GO or its overlap with high-intensity PEG and the low loading ratio [5,39]. Nevertheless, these results indicated that GO reinforcing does not affect the PEG crystal structure [7,40].

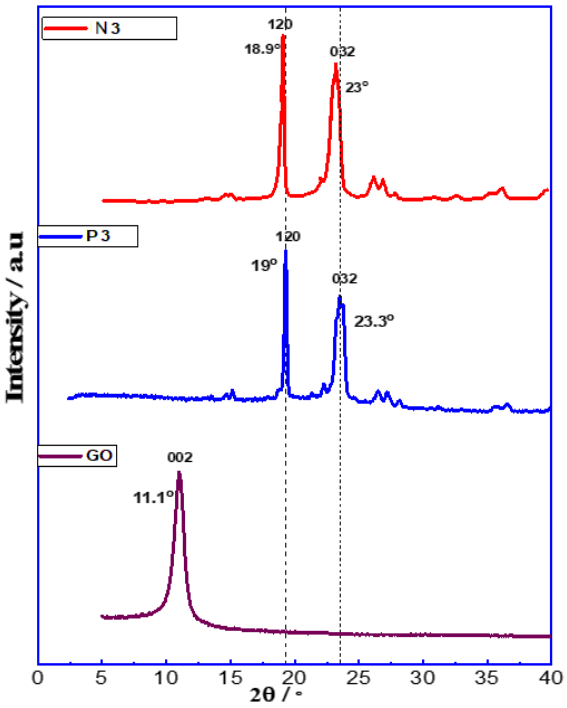

Figure 2. XRD patterns of GO and P3 and N3 nanocomposites.

Figure 3 shows the UV-visible absorption spectra of the PVA/$PEG_{4k, 8k, 20k}$ blends and their hybrid nanocomposites with GO recorded at RT in the wavelength region of 200–1100 nm. At 230 nm, the absorption peak corresponded to the transition of plasmonic π-π* (C=C) of as-prepared GO. At around 300 nm, a shoulder related to the transition of n-π* (C=O) was observed [41]. In addition, the strong absorption band at 200–300 nm could be caused by the covalent bonding interactions or π–π stacking between the GO and blended polymers. Therefore, in the visible light band, the absorption of GO was greater than that of blended polymers. The slow re-shift of the plasmonic peak was observed from 230 to 270 nm, and this process was accelerated by the increasing reaction time [42]. This shift could be due to an increase in the percentage of sp^2-hybridized carbon atoms [41].

The optical transmittance spectra of the PVA/$PEG_{4k, 8k, 20k}$ blends and their hybrid nanocomposites with GO are revealed in Figure 4. PVA/PEG_1 displayed an average optical transmittance of 87%–90% in the UV-vis-NIR radiation region. This behavior was reduced to about 77–80% after the increase in the Mw of PEGs and GO. This reduction behavior could be related to the sample's surface nature, which absorbed most of the incident light. At 200 nm, the peak transition of plasmonic π-π* (C=C) was responsible for the peak absorption of synthesis GO. Meanwhile, the presented shoulder was corresponded to n-π* (C=O) transition at around 270 nm [41]. The slow re-shift of the plasmonic peak was observed from 200 to 270 nm, and this process was accelerated by the increasing reaction time [42]. This shift could be attributed to an increase in the percentage of sp^2-hybridized carbon atoms [41]. Therefore, in the visible light band, the absorption of GO was greater than that of blended polymers.

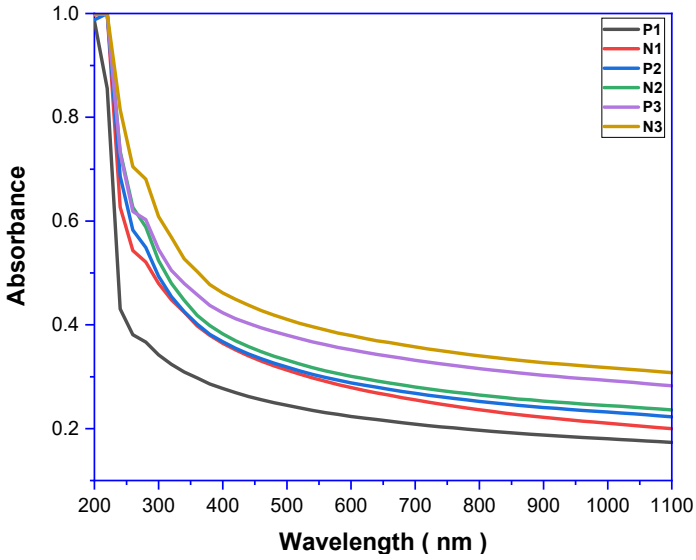

Figure 3. Absorbance spectra of blended polymers and nanocomposites.

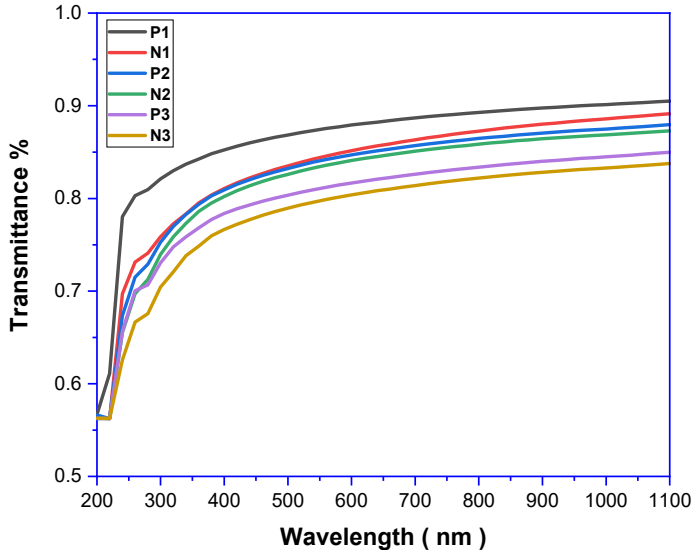

Figure 4. Transmittance spectra of blended polymers and nanocomposites.

The absorption coefficient (α) and the energy of the photon ($h\nu$) of PVA/$PEG_{4k, 8k, 20k}$ blends and their nanocomposites with GO are shown in Figure 5. α had the lowest values at low energy points, and this phenomenon could be related to the slight possibility of electron transition. At high energies, the electron absorption was excellent, with $\alpha \leq 10^4$ cm^{-1}. This finding could be related to the high probability of indirect electronic transition. This result agreed with a previous study on GO nanosheets [7].

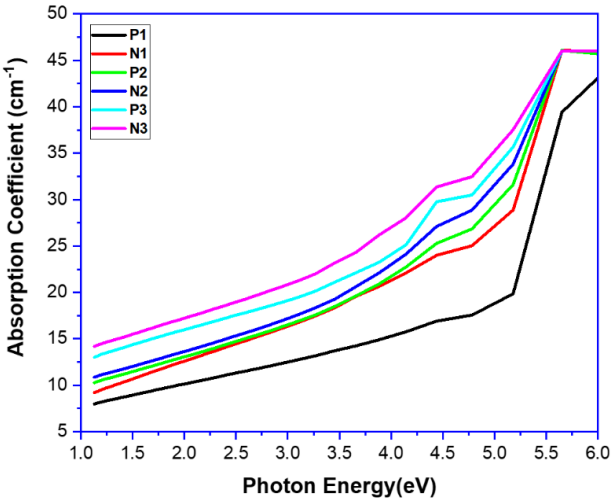

Figure 5. Absorption coefficients of blended polymers and nanocomposites.

The optical energy gap (E_g^{opt}) of nanocomposites for direct and indirect transitions was calculated using Eq 3, and the results are shown in Figures 6 and 7 and Table 2. E_g^{opt} was significantly reduced in both transitions with the change of PEG Mw and GO additive. This finding can be attributed to the increase in the disorder degree caused by the increase in Mw. GO is an essential factor in tuning the bandgap and contributed by significantly reducing the energy gap. The disorder degree in the polymer causing a reduction in the optical gap agreed with a previous study [7].

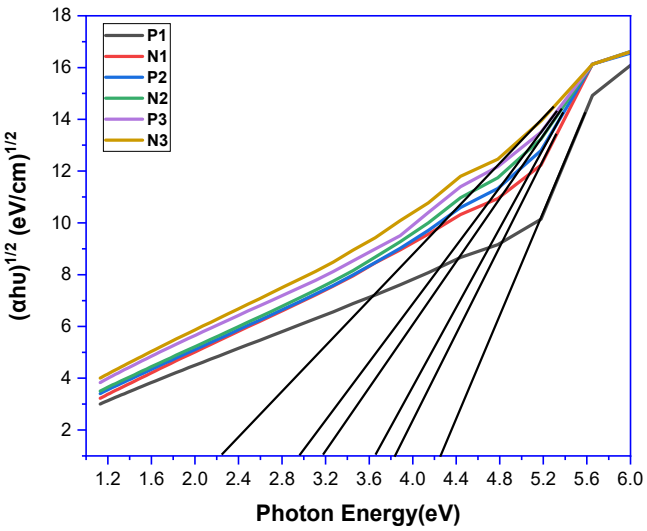

Figure 6. Optical energy gaps of the allowed transition and the photon energy (hν) of blended polymers and nanocomposites.

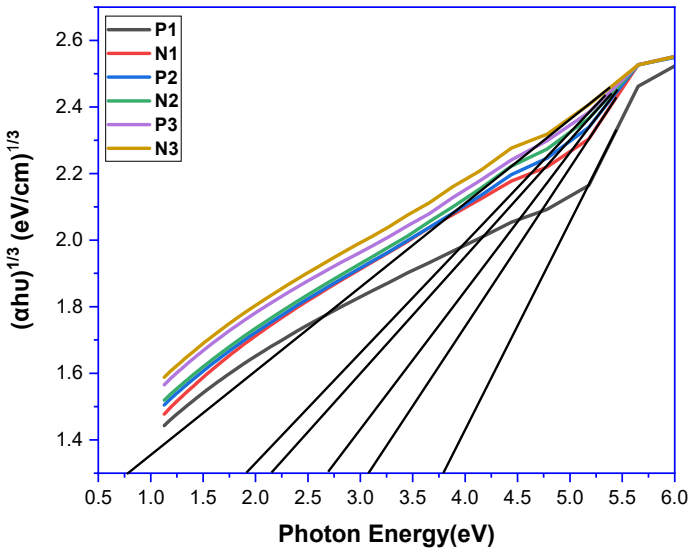

Figure 7. Optical energy gaps of the allowed transition and the photon energy (hν) of blended polymers and nanocomposites.

Table 2. Optical energy gaps of the indirect transitions of polymers and nanocomposites.

Sample	Allowed (eV)	Forbidden (eV)
P1	4.22	3.8
N1	3.81	3.1
P2	3.62	2.7
N2	3.19	2.15
P3	2.9	1.9
N3	2.21	0.8

Figure 8 illustrates the calculated refractive index values using Eq 4. The refractive index increased with the upward change of PEG Mws and GO additive in all regions, resulting in the condensation polymer chains and hydrogen intermolecular interactions among the C–O groups of GO through the O–H group of PEG. The UV region showed the highest refractive index value, with a maximum of 2.54. Linear relationships were found between the refractive index and Mw [33].

Figure 9 shows the variation of the polarizability of PVA/PEG$_{4k,\ 8k,\ 20k}$ blends and their nanocomposites with GO with photon energy calculated from Eq 8. The polarizability exhibited a similar behavior to the refractive index. Therefore, increasing the polarization produced a great refractive index, and materials without polarization do not exhibit any variation in the light speed. Consequently, the refractive index was equivalent to 1 [7].

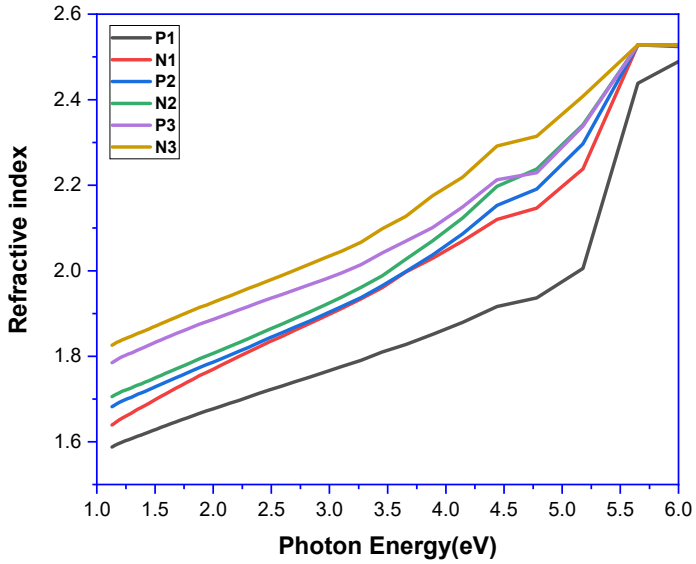

Figure 8. Refractive index of blended polymers and nanocomposites.

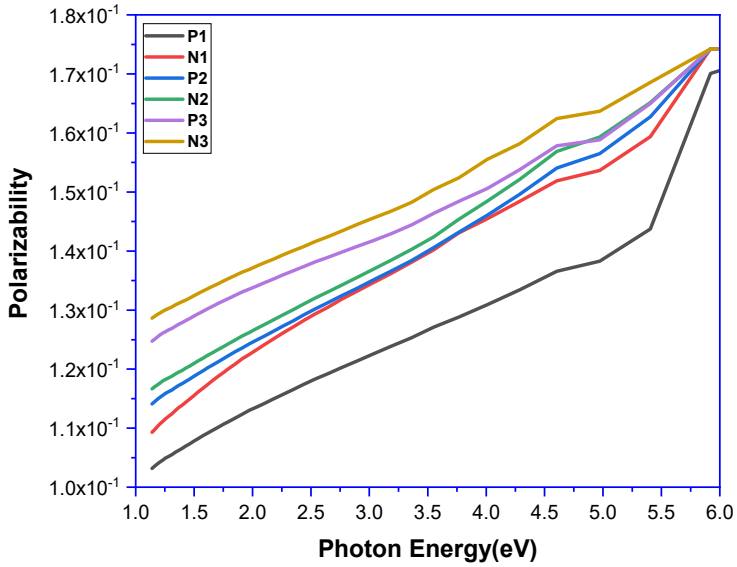

Figure 9. Polarizability of blended polymers and nanocomposites.

Equation 5 was used to calculate the extinction coefficient, as shown in Figure 10. A reduction in extinction coefficient was observed at the low photonic energy values. As a result, the energies near the edge of the total absorption were increased. In addition, the extinction coefficient was improved with the increase in PEG Mw and GO loading for the whole region.

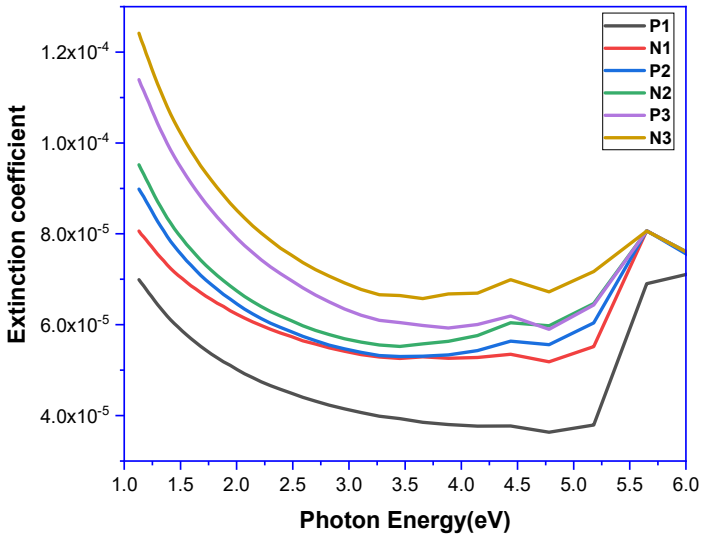

Figure 10. Extinction coefficients of blended polymers and nanocomposites.

The real part value presented a gradual improvement with increasing the light speed of the samples, and the imaginary part showed that the electric field through dipole motion absorbed the dielectric energy. Figures 11 and 12 illustrate the results for the real dielectric constant (ε_r) and imaginary dielectric constant (ε_i) measured using Eqs 6 and 7, respectively. The real dielectric constant was calculated for material polarization. A reduction was observed in the photonic energy, followed by an increase in the energies close to the fundamental absorption edge. The real part for blended polymers increased with the upward change of Mw and GO additive in all regions. The improvement in the polymeric dielectric constant of blends revealed an improvement in the charges inside the polymers. As exhibited in Figure 12, the imaginary dielectric constant showed similar behavior but lower values than the real dielectric constant.

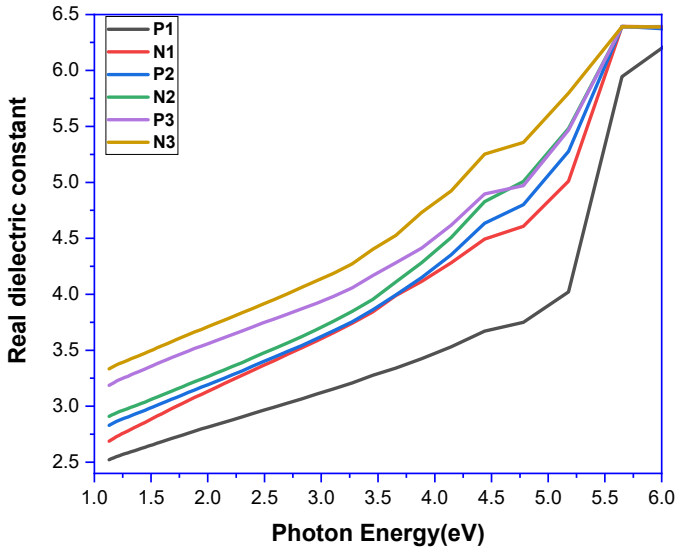

Figure 11. Real dielectric constants of blended polymers and nanocomposites.

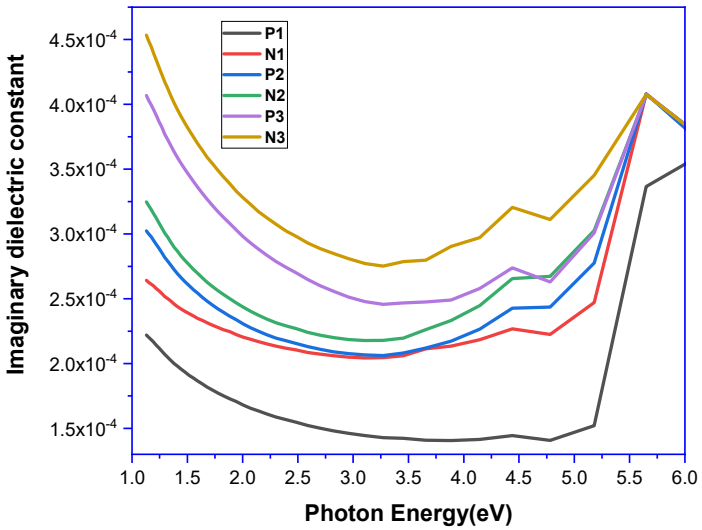

Figure 12. Imaginary dielectric constants of blended polymers and nanocomposites.

Figure 13 illustrates the change in the optical conductivity (σ) calculated using Eq 9. The results showed that σ was dependent on the absorption coefficient and grew sharply at high energy values. This finding indicated transmittance inside the visible and near-infrared regions of the nanocomposite's optical conductivity spectra. This behavior could be attributed to the charge transfer complex that originated from the impact of nano additives on the optical conductivity.

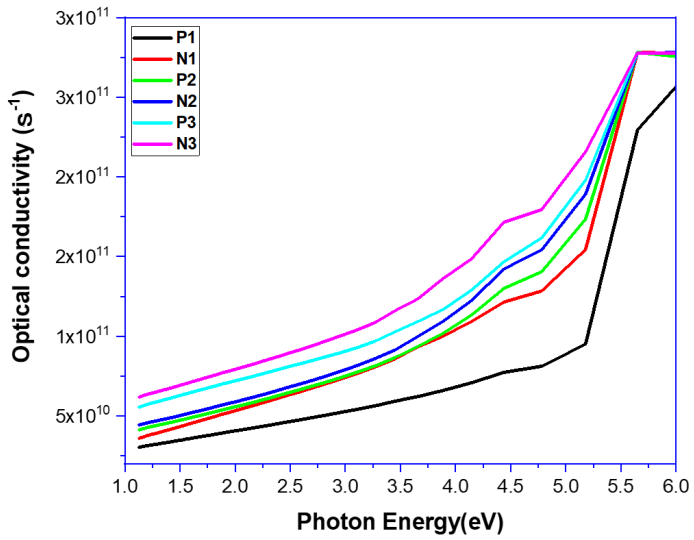

Figure 13. Optical conductivity of blended polymers and nanocomposites.

The dielectric loss angle of samples was calculated using Eq 11 and is presented in Figure 14. A slow reduction was observed for the low photonic results. The value slowly decreased and then gradually increased at the energies close to the fundamental absorption edge. Owing to the high value of the real dielectric constant and low loss established at RT with high photon energy, the polymer nanocomposites can be used as candidate materials for electronic devices.

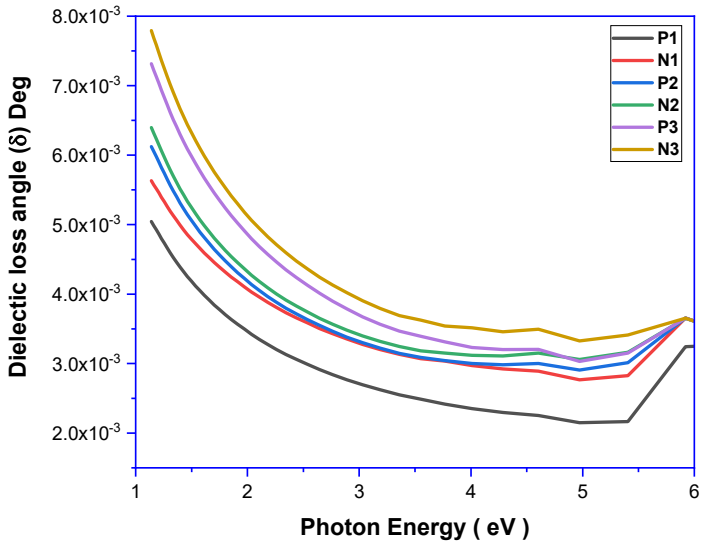

Figure 14. Dielectric loss angle of blended polymers and nanocomposites.

Figure 15 shows the microscopic images of the PVA/$PEG_{4k,\ 8k,\ 20k}$ blends and nanocomposites at 100× magnification. The images showed the good homogeneity of the polymer samples and the fine dispersion of graphene oxide nanosheets. Furthermore, the increase in the Mw of polyethylene glycol improved the interfacial interactions between the two polymers and the GO nanosheets. Samples N2 and N3 showed better and smoother surfaces that could lead to better homogeneity between the polymers compared to N1. The images supported the findings from the FTIR spectra; that is, strong interfacial interaction occurred due to the increase in the Mw of PEG polymers. Moreover, GO usually has a wide range of particle sizes, from nanometers to several microns. Therefore, the micron particles attracted by van der Walls forces could exhibit some aggregation. Nevertheless, the samples exhibited a fine and accessible dispersion of GO nanosheets in the polymer matrix [7].

Figure 16 illustrates the morphologies of the samples examined by SEM. According to the SEM image in Figure 16a, the blended polymers showed a homogeneous surface. The surface behavior significantly changed with GO addition, and a fine spread of GO was found on the surfaces of the nanocomposites. This result demonstrated the advanced homogeneity mechanism of GO with some aggregates. In addition, the surface smoothness increased with the Mw of the polymer in the matrixes [26], as revealed in Figure 16b–d.

The relation between the radiation attenuation (N) and the number of radiation particles (labeled as N/N_o ratio) was recorded during a specific time (N_o) and plotted with the increasing Mws of PEGs as shown in Figure 17. A substantial absorption of radiation was observed with the increase in the Mws of the PEGs in the matrix compared with that in the blended polymers. In addition, GO's high stability under some harsh conditions and the presence of different oxygenated and polar groups in its large surface area played significant roles in the high radiation sorption capacity of the samples [6]. This finding was in agreement with previous studies [6,43], which considered that GO could simply desorb and adsorb radionuclides without requiring another external compound. Therefore, this compound can be used to remove heavy metal ions from wastewater and for waste management applications, such as landfilling chemicals, nuclear waste and radioactive waste [6,7,9,12,44].

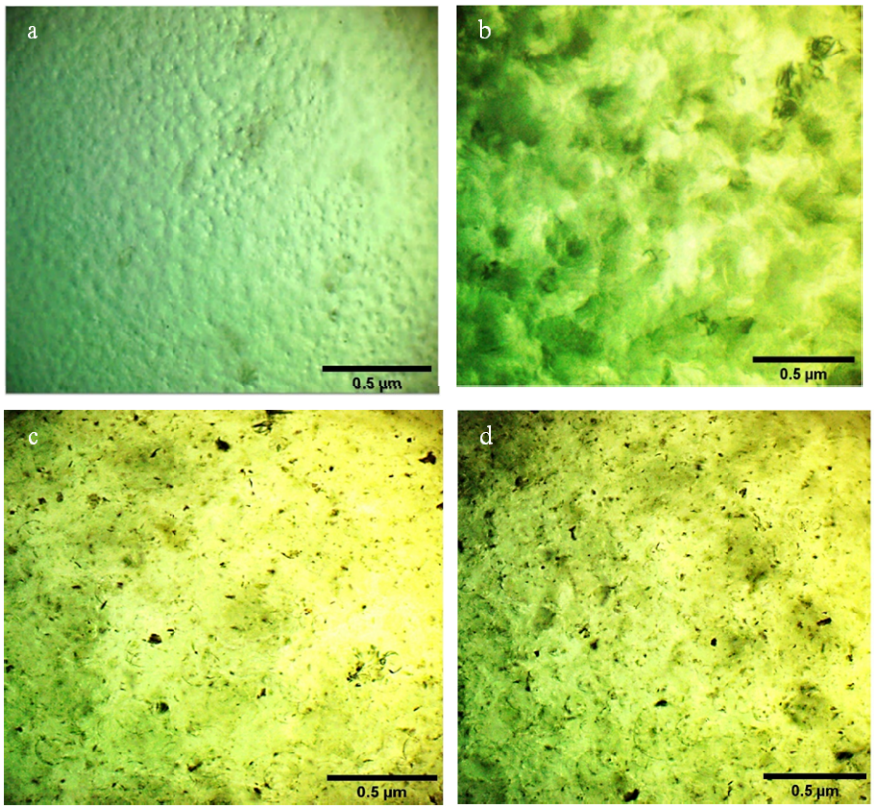

Figure 15. Optical microscopic images of (a) P1 blends and (b) N1, (c) N2 and (d) N3 nanocomposites at 100× magnification.

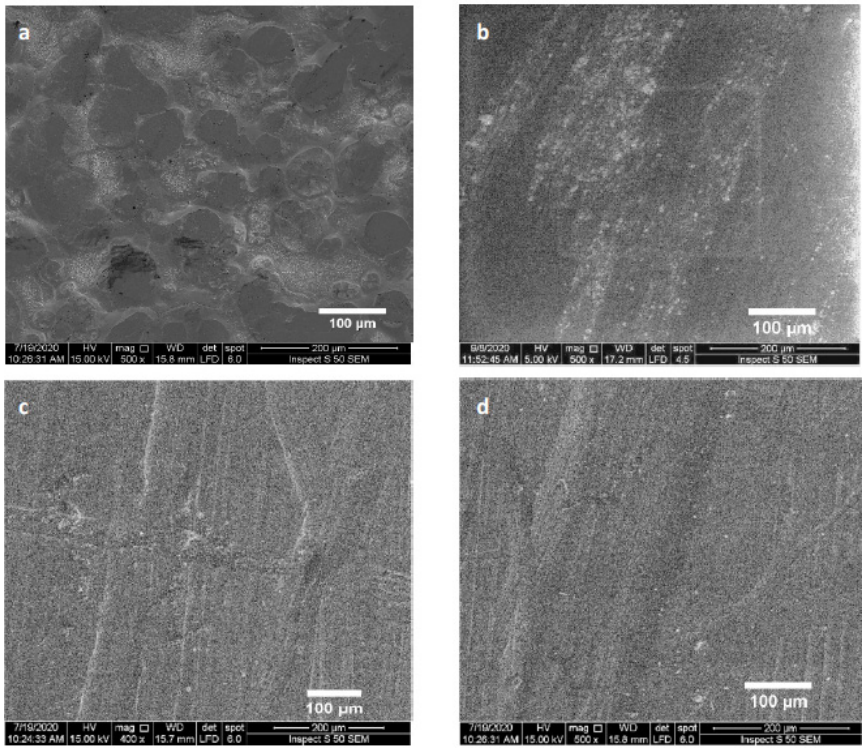

Figure 16. SEM images of (a) P1 polymer blend and (b) N1, (c) N2 and (d) N3 nanocomposites.

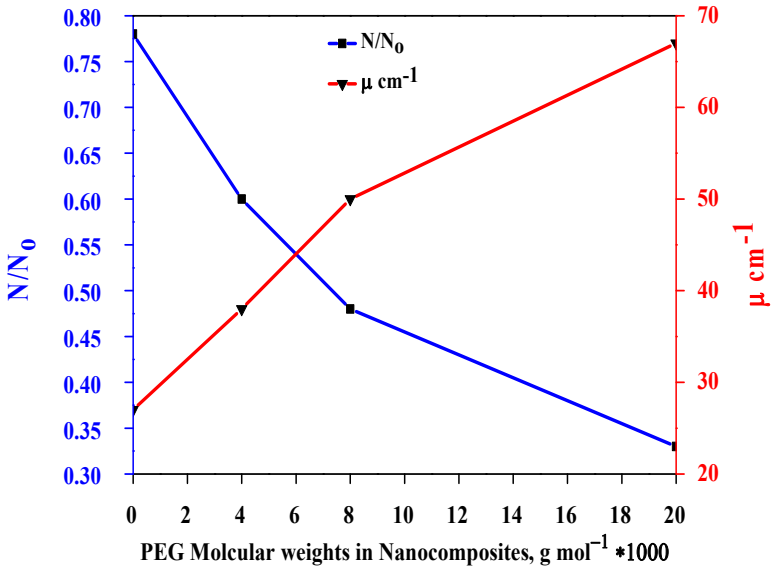

Figure 17. Relation between radiation attenuation (N) and the number of radiation particles (N_o) with the attenuation coefficient of radiation vs. the PEG Mws of nanocomposites.

4. Conclusions

Nanocomposites were successfully fabricated using a developed method of aquatic mixing-sonication-casting. The effects of PEG Mw on the structures and optical properties of these nanocomposites were investigated. FTIR spectroscopy revealed strong interfacial interaction peaks in the polymers with the increasing Mws of PEG. XRD supported these results. SEM and OM images showed better and smoother surfaces of the samples after the increase in the Mws of PEG. In addition, the fine dispersion of nanoscale GO was observed, and some aggregation of micron-sized GO was found in several samples. Increasing the Mw and GO nanosheets significantly enhanced the absorption of UV waves and helped maintain good optical transmittance values (90%–77%). In addition, PEG Mw and GO loading significantly improved optical properties such as absorbance, dielectric constants (real and imaginary) and absorption coefficient constants up to 75%, 40%, 120% and 77%, respectively. The indirect transition optical energy gap (allowed and forbidden) was improved up to 90% and 375%, respectively, by reducing the values of the above indexes with the upward change of Mw and GO additive in all regions. The same behavior was observed for the optical absorption edge. In addition to the contribution of GO in the polymer matrix, the results also revealed the substantial absorption of radiation with the increasing Mws of the PEGs in the matrix. This study showed the importance of the Mw of polymers and its effect on the results. Based on all the findings, these nanomaterials are suitable for various applications, such as UV protection, solar cells, radiation shields and drug storage.

Acknowledgments

The authors would like to thank the Department of Material Science and Engineering at the University of Sheffield, UK; the Department of Physics, University of Babylon; Al-Mustaqbal

University College, Iraq; and the Center of Nanomaterials in the Ministry of Higher Education and Scientific Research, Iraq for their support.

Conflict of interest

The authors declare no conflict of interest.

References

1. El-Naggar ME, Ali OAA, Saleh DI, et al. (2022) Nanoarchitectonics of hydroxyapatite/molybdenum trioxide/graphene oxide composite for efficient antibacterial activity. *J Inorg Organomet Polym* 32: 399–411. https://doi.org/10.1007/s10904-021-02109-8
2. Pan X, Debije MG, Schenning APHJ, et al. (2021) Enhanced thermal conductivity in oriented polyvinyl alcohol/graphene oxide composites. *ACS Appl Mater Interfaces* 13:28864–28869. https://doi.org/10.1021/acsami.1c06415
3. Kasim H, Yazici M (2019) Electrical properties of graphene/natural rubber nanocomposites coated nylon 6.6 fabric under cyclic loading. *Period Polytech-Chem* 63:160–169. https://doi.org/10.3311/PPch.12122
4. Akram N, Saeed M, Usman M, et al. (2021) Influence of graphene oxide contents on thmechanical behavior of polyurethane composites fabricated with different diisocyanates. *Polymers* 13:1–16. https://doi.org/10.3390/polym13030444
5. Al-Bermany E, Chen B (2021) Preparation and characterisation of poly(ethylene glycol)-adsorbed graphene oxide nanosheets. *Polym Int* 70: 341–351. https://doi.org/10.1002/pi.6140
6. Sánchez-García I, Núñez A, Bonales LJ, et al (2019) Study of the adsorption capacity of grapinhene oxide under gamma radiation different media. *Radiat Phys Chem* 165: 1–24. https://doi.org/10.1016/j.radphyschem.2019.108395
7. Kadhim MA, Al-Bermany E (2021) New fabricated PMMA-PVA/graphene oxide nanocomposites: Structure, optical properties and application. *J Compos Mater* 50: 2793–2806. https://doi.org/DOI: 10.1177/0021998321995912
8. Cui M, Park S-J, Kim S (2021) Carboxylated group effect of graphene oxide on capacitance performance of Zr-based metal organic framework electrodes. *J Inorg Organomet Polym Mater* 31: 1939–1945. https://doi.org/10.1007/s10904-021-01935-0
9. Carey T, Williams CD, Mcarthur DJ, et al. (2018) Removal of Cs, Sr, U and Pu species from simulated nuclear waste effluent using graphene oxide. *J Radioanal Nucl Chem* 317: 93–102. https://doi.org/10.1007/s10967-018-5931-0
10. Zhang X, Zhang W, Dong H, et al. (2021) The influence of the structure of pyromellitic acid on the luminescence intensity of graphene oxide/rare earth complexes hybrid materials. *J Inorg Organomet Polym Mater* 31: 3740–3748. https://doi.org/10.1007/s10904-021-01962-x
11. Abdul kadhim M, Al-bermany E (2020) Enhance the electrical properties of the novel fabricated PMMA-PVA/graphene based nanocomposites. *J Green Eng* 10: 3465–3483.

12. Harish Kumar A, Ahamed MB, Deshmukh K, et al. (2021) Morphology, dielectric and EMI shielding characteristics of graphene nanoplatelets, montmorillonite nanoclay and titanium dioxide nanoparticles reinforced polyvinylidenefluoride nanocomposites. *J Inorg Organomet Polym Mater* 31: 2003–2016. https://doi.org/10.1007/s10904-020-01869-z
13. Lv H, Guo Y, Yang Z, et al. (2017) A brief introduction to the fabrication and synthesis of graphene based composites for the realization of electromagnetic absorbing materials. *J Mater Chem C* 5: 491–512. https://doi.org/10.1039/C6TC03026B
14. Al-shammari AK, Al-Bermany E (2021) New fabricated (PAA-PVA/GO) and (PAAm-PVA/GO) nanocomposites: Functional groups and graphene nanosheets effect on the morphology and mechanical properties. *J Phys Conf Ser* 1973: 012165. https://doi.org/10.1088/1742-6596/1973/1/012165
15. Gao S, Liu Z, Yan Q, et al. (2021) Facile synthesis of polypyrrole/reduced graphene oxide composite hydrogel for Cr(VI) removal. *J Inorg Organomet Polym Mater* 31: 3677–3685. https://doi.org/10.1007/s10904-021-02037-7
16. AI Abdelamir, Al-Bermany E, Hashim FS (2019) Enhance the optical properties of the synthesis PEG/graphene-based nanocomposite films using GO nanosheets. *JPCS* 1294: 022029. https://doi.org/10.1088/1742-6596/1294/2/022029
17. Chem P, Phys C, Tozzini V, et al. (2013) Prospects for hydrogen storage in graphene. *Phys Chem Chem Phys* 15: 80–89. https://doi.org/10.1039/c2cp42538f
18. Al-nesrawya SH, Mohseenb MJ, Al-Bermany E (2020) Reinforcement the mechanical properties of (NR50/SBRs50/ OSP) composites with oyster shell powder and carbon black. *IOP Conf Ser Mater Sci Eng* 871: 012060. https://doi.org/10.1088/1757-899X/871/1/012060
19. Aldulaimi NR, Al-Bermany E (2021) New fabricated UHMWPEO-PVA hybrid nanocomposites reinforced by GO nanosheets: Structure and DC electrical behaviour. *JPCS* 1973: 012164. https://doi.org/10.1088/1742-6596/1973/1/012164
20. Devangamath SS, Lobo B, Masti SP, et al. (2020) Thermal, mechanical, and AC electrical studies of PVA–PEG–Ag_2S polymer hybrid material. *J Mater Sci Mater Electron* 31: 2904–2917. https://doi.org/10.1007/s10854-019-02835-3
21. Al-shammari AK, Al-Bermany E (2022) Polymer functional group impact on the thermo-mechanical properties of polyacrylic acid, polyacrylic amide- poly(vinyl alcohol) nanocomposites reinforced by graphene oxide nanosheets. *J Polym Res* 29: 351. https://doi.org/10.1007/s10965-022-03210-3
22. Rashid A-KJ, Jawad ED, Kadem BY (2011) A study of some mechanical properties of Iraqi palm fiber-PVA composite by ultrasonic. *Eur J Sci Res* 61: 203–209.
23. Alla SGA, El-din HMN, El-naggar AWM (2006) Electron beam synthesis and characterization of poly(vinyl alcohol)/montmorillonite nanocomposites. *J Appl Polym Sci* 102: 1129–1138. https://doi.org/10.1002/app.24370
24. Al-Owaedi OA, Khalil TT, Karim SA, et al. (2020) The promising barrier: Theoretical investigation. *Syst Rev Pharm* 11: 110–115. https://doi.org/10.31838/srp.2020.5.18
25. Li D, Sur GS (2014) Composites prepared by penetrating poly(ethylene oxide) chains into graphene interlayers. *Macromol Res* 22: 113–116. https://doi.org/10.1007/s13233-014-2021-1

26. Al-Abbas SS, Ghazi RA, Al-shammari AK, et al. (2021) Influence of the polymer molecular weights on the electrical properties of Poly(vinyl alcohol)–Poly(ethylene glycols)/Graphene oxide nanocomposites. *Mater Today Proc* 42: 2469–2474. https://doi.org/10.1016/j.matpr.2020.12.565
27. Morsi MA, Abdelghany AM (2017) UV-irradiation assisted control of the structural, optical and thermal properties of PEO/PVP blended gold nanoparticles. *Mater Chem Phys* 201: 100–112. https://doi.org/10.1016/j.matchemphys.2017.08.022
28. Yang Z, Peng H, Wang W, et al. (2010) Crystallization behavior of poly(ε-caprolactone)/layered double hydroxide nanocomposites. *J Appl Polym Sci* 116: 2658–2667. https://doi.org/10.1002/app
29. Basha SKS, Kumar KV, Sundari GS, et al. (2018) Structural and electrical properties of graphene oxide-doped PVA/PVP blend nanocomposite polymer films. *Adv Mater Sci Eng* 2018: 1–11. https://doi.org/10.1155/2018/4372365
30. Falqi FH, Bin-dahman OA, Hussain M, et al. (2018) Preparation of miscible PVA/PEG blends and effect of graphene concentration on thermal, crystallization, morphological, and mechanical properties of PVA/PEG (10 wt%) blend. *Int J Polym Sci* 2018: 1–10. https://doi.org/10.1155/2018/8527693
31. Li C, Xiang M, Ye L (2016) Intercalation behavior and orientation structure of graphene oxide/polyethylene glycol hybrid. *RSC Adv* 6: 72193–72200.
32. Xiong J, Li S, Li Y, et al. (2020) Fluorescent aptamer-polyethylene glycol functionalized graphene oxide biosensor for profenofos detection in food. *Chem Res Chinese Univ* 36: 787–794. https://doi.org/10.1007/s40242-019-9257-4
33. Ingham JD, Lawson DD (1965) Refractive index-molecular weight helatlonships. *J Polym Sci* A 3: 2707–2710. https://doi.org/10.1002/pol.1965.100030728
34. Kittle C (2005*) Introduction to Solid State Physics*, 8 Eds., John Wiley and Sons Inc.
35. Tintu R, Saurav K, Sulakshna B, et al. (2010) $Ge_{28}Se_{60}Sb_{12}$/PVA composite films for photonic applications. *J Non-Oxide Glasses* 2: 167–174.
36. Hasnat A, Podder J (2012) Dielectric properties of spray pyrolized Aluminum doped Cadmium sulfide (Al-doped CdS) thin films. *Int J Phys Sci* 7: 6158–6161. https://doi.org/10.5897/IJPS12.539
37. Abdelamir AI, Al-Bermany E, Hashim FS (2020) Important factors affecting the microstructure and mechanical properties of PEG/GO-based nanographene composites fabricated applying assembly-acoustic method. *AIP Conf Proc* 020110. https://doi.org/10.1063/5.0000175
38. Pulst M, Samiullah MH, Baumeister U, et al. (2016) Crystallization of poly(ethylene oxide) with a well-defined point defect in the middle of the polymer chain. *Macromolecules* 49: 6609–6620. https://doi.org/10.1021/acs.macromol.6b01107
39. Han Y, Wang T, Gao X, et al. (2016) Preparation of thermally reduced graphene oxide and the influence of its reduction temperature on the thermal, mechanical, flame retardant performances of PS nanocomposites. *Compos Part A Appl Sci Manuf* 84: 336–343. https://doi.org/10.1016/j.compositesa.2016.02.007
40. Fu Y, Xiong W, Wang J, et al. (2017) Polyethylene glycol based graphene aerogel confined phase change materials with high thermal stability. *J Nanosci Nanotechnol* 18: 3341–3347. https://doi.org/10.1166/jnn.2018.14635

41. Aldulaimi NR, Al-Bermany E (2022) Tuning the bandgap and absorption behaviour of the newly-fabricated Ultrahigh Molecular weight Polyethylene Oxide-Polyvinyl Alcohol/Graphene Oxide hybrid nanocomposites, *Polym Polym Compos* 30: 096739112211121. https://doi.org/10.1177/09673911221112196
42. Li D, Müller MB, Gilje S, et al. (2008) Processable aqueous dispersions of graphene nanosheets. *Nat Nanotechnol* 3: 101–105. https://doi.org/10.1038/nnano.2007.451
43. Kyzas GZ, Deliyanni EA, Matis KA (2014) Graphene oxide and its application as adsorbent to wastewater treatment. *J Chem Technol Biotechnol* 89: 196–205. https://doi.org/10.1002/jctb.4220
44. Wang F, Li H, Liu Q, et al. (2016) A graphene oxide/amidoxime hydrogel for enhanced uranium capture. *Sci Rep* 6: 1–8. https://doi.org/10.1038/srep19367

AIMS Press